Int. J. Electrochem. Sci., 7 **(2012)** 12207 - 12217

International Journal of
ELECTROCHEMICAL
SCIENCE
www.electrochemsci.org

Fabrication of Honeycomb Gold Arrays for Enhancement of Electrochemical Performance

Yanhua Li[1, 2,*], *Dongming Zeng*[2], *Qiyuan Chen*[2], *Shiying Zhang*[1], *Qumin Yu*[1], *Difa Xu*[1]

[1] Department of Biological and Environmental Science, Changsha University, Changsha 410003, China
[2] College of Chemistry and Chemical Engineering, Central South University, Changsha 410083, China
[*]E-mail: liyanhua12@yahoo.com.cn

Received: 5 October 2012 / *Accepted:* 29 October 2012 / *Published:* 1 December 2012

Hexagonally close-packed polystyrene (PS) nanospheres assembled onto gold films substrates were used to as templates to fabricate honeycomb gold arrays. Gold was electrodeposited in the interstitial voids surrounded by the PS sphere cores and extraction of the PS sphere cores with toluene resulted in the formation of honeycomb gold arrays. The thickness of the arrays can be altered by varying the deposition potential and the concentration of the gold plating solution. The morphology and the dimension were characterized by atomic force microscopy and cyclic voltammetry. The enhanced surface area of gold surface for functionalization may render substrates decorated with these arrays as new electrochemical sensors and used in DNA analysis.

Keywords: Polystyrene nanospheres; Electrodeposition; Honeycomb gold arrays; Electrochemical sensors; DNA.

1. INTRODUCTION

There is currently a great deal of interest in template-directed synthesis of nanoporous materials ranging from microporous to macroporous, and further to hierarchical porous structures [1]. Highly ordered two-dimensional (2-D) colloidal crystals and three-dimensional (3-D) colloidal crystals constructed from various colloidal spheres, such as silica and latex particles have served as effective templates for preparing porous materials. In the face-centered cubic structure of colloidal crystal template, spheres occupy 74% in volume of the unit cell [2]. The interstices of the template could be filled with another material via different routes, such as hydrothermal synthesis [3], chemical bath deposition [4], and electrodeposition [5]. After removing the colloidal template chemically or thermally, a wide variety of porous materials, such as metal [6, 7], inorganic oxide [2, 5, 8], carbon [9,

10], semiconductor [11], and organic polymer [12], are produced. These porous materials could find potential applications in areas as diverse as catalysis, sensors, photonic crystals, and nano-electronics. Different types of porous materials such as honeycomb films, nano-triangles and hollow sphere arrays could be fabricated via colloidal crystal template-assisted methods. Nanoporous materials possess high surface areas and the net surface area can reach several square meters for a thin film only one centimeter across [13].

Due to the enhanced surface area, many porous electrodes have been found to greatly increase the sensitivity of the electrochemical signal [14]. Catalytic applications may also benefit from the open porous structure of these materials with increased surface area [13, 15]. Besides, this kind of structure can also be regarded as a good candidate for biosensors such as glucose detection [16, 17], the direct electron transfer of hemoglobin [18] and the adsorption kinetics and biocatalytic properties of cytochrome c [19]. Recently, macroporous three-dimensional gold modified electrodes have also been used as immunosensor development [20, 21]. Compared with respective nonporous electrodes, macroporous gold modified electrodes greatly increase sensing enhancement. However, to the best of our knowledge, little attention has been devoted to macroporous two-dimensional gold for DNA analysis to improve sensitivity of DNA hybridization reactions.

In the present work, 2-D hexagonally close-packed PS nanospheres were first formed on gold films substrates by evaporating the solvent at room temperature. Honeycomb gold arrays were then constructed via electrodeposition within the interstitial voids of 2D nanospheres, followed by extraction of the PS particles with toluene. Porous materials including honeycomb gold arrays constructed via electrodeposition are promising and readily to produce because the involved electrochemical techniques are simple, sensitive, and inexpensive to implement [22]. Moreover, thickness of electrodeposited porous materials can be easily controlled by changing deposition variables, such as voltage or current density, pH value and concentration of the solution [1]. The resultant honeycomb gold arrays with different thickness can be used as electrochemical sensors to promote electron transfer reactions between the redox species with the underlying electrode and used in DNA analysis to improve sensitivity of DNA hybridization reactions.

2. EXPERIMENTAL SECTION

2.1. Materials.

PS nanospheres with a diameter of 600 nm were acquired from Interfacial Dynamics Inc. (Portland, OR, U. S. A.). A ferrocene-terminated alkanethiol, 6-ferrocenyl-1-hexanethiol, was obtained from Dojindo (detailed location, Japan). Gold tetrachloride was purchased from Sinopharm Chemical Reagent Co. LTD (Vendor info. in China). Ethylenediaminetetraacetic acid (EDTA) and Tris-HCl were all purchased from Beijing Chemical Reagents Company (Beijing, China). Mercaptohexanol (MCH) was obtained from Aldrich Chemicals. All other chemicals were of reagent grade. ODN capture probes with their 5’ ends modified with hexylthiol groups and detection probes with their 3’ ends attached to a thiol linker were both obtained from Sangon Co., LTD (Shanghai, China). Sequences of the capture and detection probes were SH-$(CH_2)_6$-5’-TTT TTG GAG CAC CCA CGT

GTC CTG GCC-3' and 5'-AGG AGA GCT CAG TTT ACT AGT GCC TTT-3'-$(CH_2)_6$-SH, respectively. Sequence of the target was 3'-GGG TGC ACA GGA CCG GTC ATA TCC TCT CGA GTC AAA TGA -5'. Fc−Mi was synthesized according to literature procedures [23]. All solutions were prepared with deionized water treated with a Millipore Milli-Q Plus 185 purification system.

2.2. Electrodes.

Au films or gold disc electrodes (CH Instruments, Austin, TX, U. S. A.) were used as the substrate for constructing 2-dimensional honeycomb gold arrays. Au films with a 50-nm thickness and a 2-nm Cr underlayer were deposited on cleaned glass slides using a sputter coater (Model 108, Kert J. Lester Inc., Clairton, PA, USA). Prior to use, the gold films substrates were cleaned with a piranha solution and rinsed with water. Gold disc electrode with a diameter of 2 mm was polished with diamond pastes and alumina slurry down to 0.05 □m on a polishing cloth (Buehler, Lake Bluff, IL), followed by sonicating in water and ethanol. Gold electrodeposition was conducted with a CHI 660B electrochemical workstation (CH Instruments, Austin, TX) in a conventional three-electrode cell. A Pt coil and an Ag/AgCl electrode were used as the counter and reference electrodes, respectively.

2.3. Instrumentation.

A CHI 660 electrochemical workstation was used to monitor the gold electrodeposition process and to obtain the voltammogram of 6-ferrocenyl-1-hexanethiol assembled onto the 2-D honeycomb gold arrays. An atomic force microscopy (PicoPlus, Agilent Technologies, CA, U. S. A.) was used to assess the quality of the PS nanospheres assembly and to characterize the honeycomb gold arrays formed under different experimental conditions.

2.4. Procedures.

2.4.1. Assembly of the PS Sphere Cores onto Substrates

The stock solution of PS nanospheres was diluted with water to a final concentration of 0.5% (V:V). Prior to use, gold films substrates were annealed in a hydrogen flame to eliminate surface contamination and to achieve a better packing of PS nanospheres. PS nanospheres were assembled onto the Au films substrates by casting 50 μL of the nanoparticle solution onto the substrates. This was followed by evaporating the solvent in a humidified chamber at room temperature. The quality of the PS nanospheres assembly was monitored by AFM (An atomic force microscopy).

2.4.2. 2-D Honeycomb Gold Arrays Formation

Gold electrodeposition was conducted in a mixed solution (pH 9.0) containing a predetermined concentration of $HAuCl_4$, 0.5 mM $(NH_4)_2SO_3$ and 2 mM potassium citrate in a conventional three-

electrode cell. Gold films or gold disc electrodes covered with the PS nanospheres assembly were used as the working electrodes. After electrodeposition, the PS cores were then extracted by sonicating the substrates in toluene for 3-4 min.

2.4.3. AFM and Electrochemical Characterizations

AFM (An atomic force microscopy) was used to characterize the honeycomb gold arrays formed under different experimental conditions. The above honeycomb gold arrays on gold disk electrodes were immersed into a 1.0 mM 6-ferrocenyl-1-hexanethiol solution dissolved in ethanol for about 20 h. This step was followed by an extensive wash with ethanol and water to rid any nonspecifically adsorbed 6-ferrocenyl-1-hexanethiol of the electrodes. The electrode was then transferred to a 0.1 M $KClO_4$ solution and characterized voltammetrically with the potential range between 0.1 and 0.6 V.

2.4.4. DNA Hybridization Investigated on the Honeycomb Gold Arrays Electrode and the Bare Gold Electrode

Honeycomb gold arrays electrodes and the bare gold electrodes were immersed into a 0.4 μM capture probe in TE (10 mM Tris-HCl and 1.0 mM EDTA) solutions for 12 h. The above electrodes were then washed with deionized water. The mixture of Fc−Mi and detection probe was prepared by mixing detection probe (100 μL, 4 mM) and Fc−Mi (100 μL, 2 μM) in centrifuging tube and was followed by shaking. The electrodes covered with capture probe were immersed into a 4 mM MCH solution dissolved in ethanol. This step was followed by a wash with deionized water. For DNA hybridization, the electrodes were soaked in TNE solutions (10 mM Tris-HCl + 1 mM EDTA + 0.1 M NaCl) containing 0.1 μM target DNA and the hybridization reactions were allowed to proceed for 3 h in the humidified Styrofoam chamber. After the surface was thoroughly rinsed with deionized water, the electrodes were immersed in the above mixture of Fc−Mi and detection probe for another 3 h. Upon completion of the two consecutive hybridization reactions, the electrodes were rinsed with water.

3. RESULTS AND DISCUSSION

Fig. 1 schematically depicts the procedures for fabrication of 2-D honeycomb gold arrays. In step 1, PS nanospheres were assembled onto the gold films by casting the nanoparticle solution and allowing the solvent to evaporate. As a reulst, hexagonally close-packed PS nanospheres were formed on the surface. In step 2， gold electrodeposition within the interstitial voids of 2D nanospheres was carried out. Finally, extraction of the PS particles with toluene resulted in the formation of the 2-D honeycomb gold arrays (step 3).

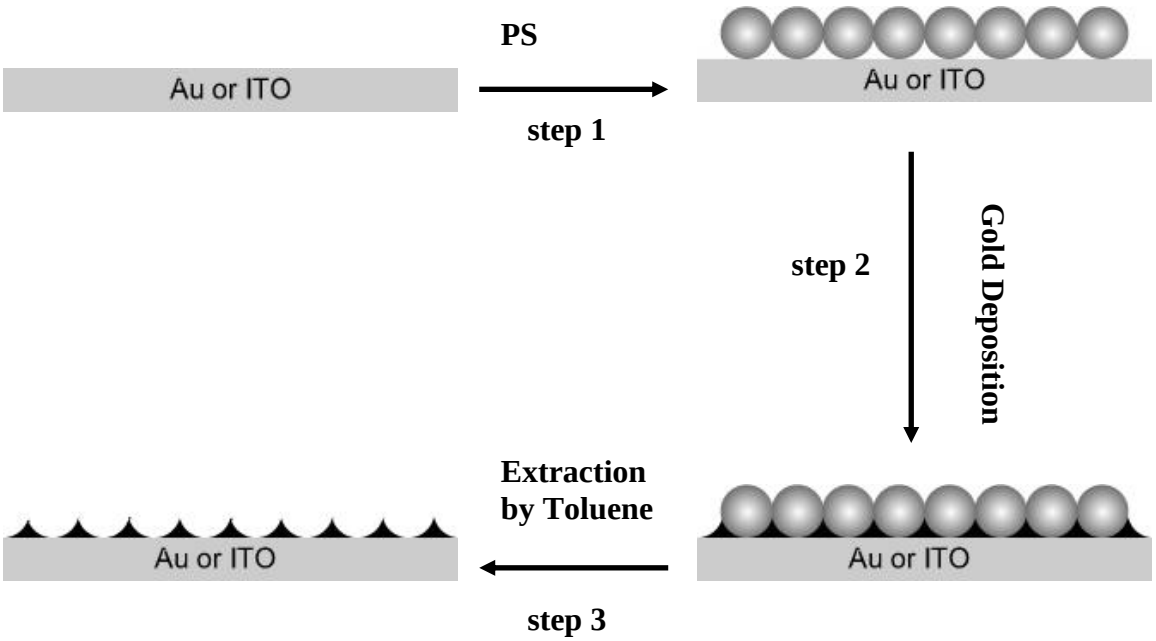

Figure 1. Schematic representation of the procedures for fabricating honeycomb gold arrays.

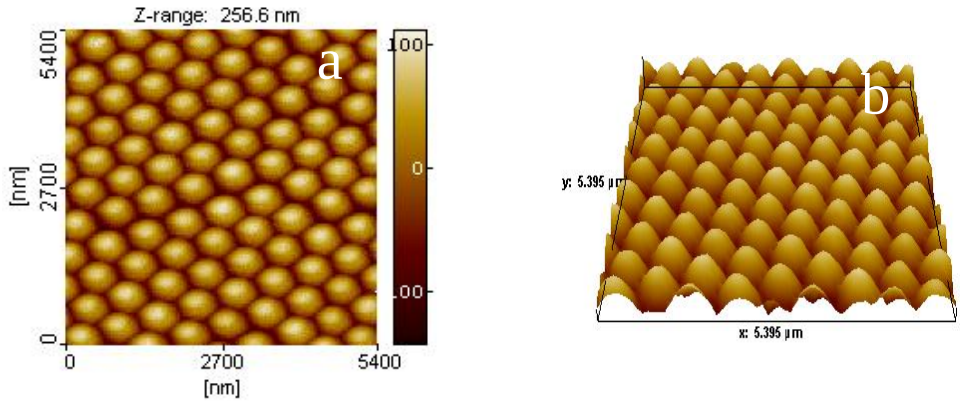

Figure 2. AFM images of hexagonally close-packed PS nanospheres assembled onto gold films. (a): two-dimensional AFM image; (b): three-dimensional AFM image.

Fig. 2 displays typical AFM images of the hexagonally close-packed PS nanospheres assembled onto the gold film (Fig. 2). AFM images were operated by Acoustic AC (AAC) mode. Well-ordered close-packed PS nanospheres were formed after solvent evaporation. The average diameter of the PS nanospheres deduced from the cross-sectional contour of the image in Fig. 2 is ca. 600 nm, which matches exactly with that of the nanospheres we purchased.

Gold deposition within the interstitial voids of 2-D PS nanospheres on gold films was conducted at a constant potential. Typical potentiostatic current transient reflects the mass-transport control for gold deposition based on the linear current density j vs. $t^{-1/2}$ plots in the insets of Fig. 3, as expected from Sand-Cottrell's equation [24]. The influence of the potential and the plating solution concentration on honeycomb gold array formation were examined. Under these conditions, the amount

of gold deposition was controlled by the charge flowing through the system. Fig. 3 shows typical AFM images of the honeycomb gold arrays formed on gold films (Fig. 3a, 3b, 3c), followed by extracting the PS cores by sonicating the substrates in toluene for 3-4 minutes.

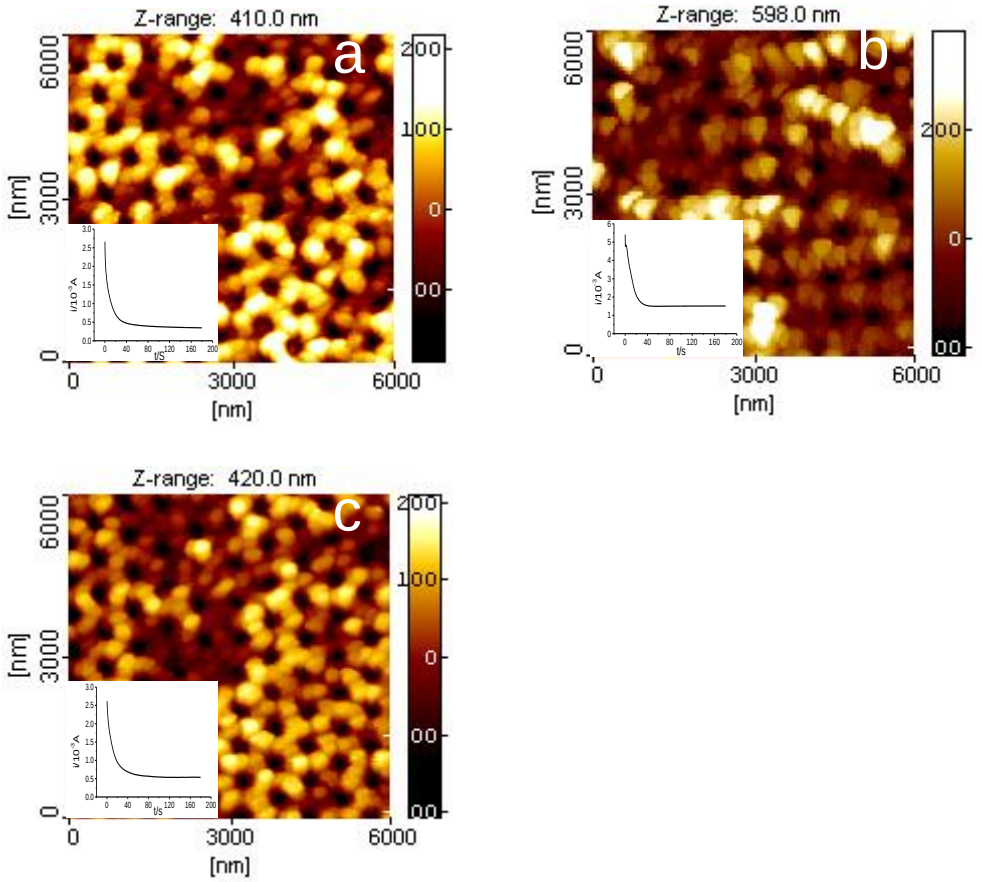

Figure 3. AFM images of the honeycomb gold arrays formed on gold films(a, b, c) at deposition potential of -0.1 V in 10 mM $HAuCl_4$ solution (a); at deposition potential of -0.8 V in 10 mM $HAuCl_4$ solution (b); at deposition potential of -0.8 V in 2.5 mM $HAuCl_4$ solution (c). The insets of Fig. show current density vs time curves for gold electrodeposition operated under different conditions.

As shown in Fig. 3a, when the deposition potential of -0.1V and the plating solution of 10 mM $HAuCl_4$ were used, the thickness of the honeycomb gold arrays is about 410 nm, which is somewhat larger than the radius of PS nanospheres assembled on the surface. With a close examination of the above image, the distance between the neighboring honeycomb gold arrays is found to be ca. 600 nm, which is in excellent accord with the diameter of close-packed PS nanospheres, indicating that the honeycomb metal arrays have not shrinked or inflated after extraction of PS cores with toluene. Hence, the size of the honeycomb gold arrays is controlled by the diameter of close-packed PS nanospheres assembled onto the surface. Deposition potential has a profound influence on the morphology of the honeycomb gold arrays formed. When the deposition potential of -0.8 V and 10 mM $HAuCl_4$ were used, the thickness of the honeycomb gold arrays is about 598 nm (Fig. 3b), which is almost the same

as the diameter of PS nanospheres assembled onto the surface. The difference in the thickness of the honeycomb gold arrays may be interpreted on the basis of different nucleation rate. Larger current density for gold deposition was obtained at -0.8 V. As a result, gold deposition may occur at the topside of the interstitial voids between close-packed PS nanospheres. Alteration of the plating solution concentration also produces significant influence on the structure of the honeycomb gold arrays. In the case of 2.5 mM $HAuCl_4$ and the deposition potential of -0.8 V, honeycomb gold arrays with a thickness of 420 nm were produced (Fig. 3c), which indicates an obvious effect on the mass transport rate control from the solution side.

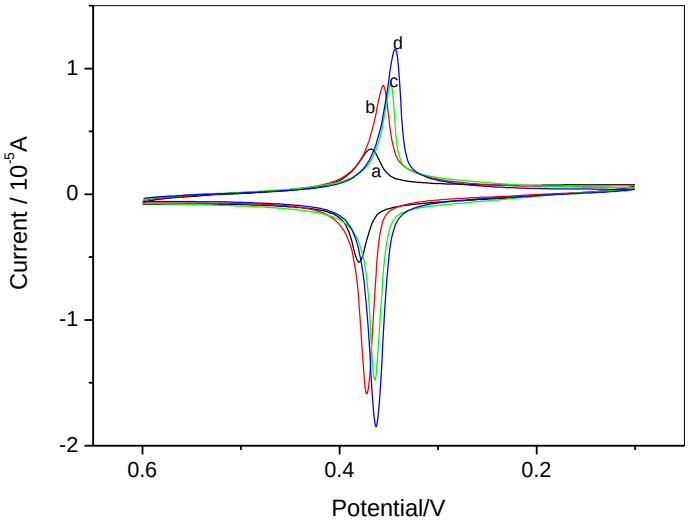

Figure 4. Cyclic voltammograms acquired at the bare gold electrode (curve a) and the honeycomb gold arrays electrode (curve b, c, d) after immersing the electrodes in an ethanol solution containing 1 mM 6-Ferrocenyl-1-hexanethiol. Curve b, c and d correspond to the electrochemical responses at the metal arrays formed at deposition potentials of -0.1 V in 10 mM $HAuCl_4$, -0.8 V in 2.5 mM $HAuCl_4$ and -0.8 V in 10 mM $HAuCl_4$, respectively. The scan rate was 0.05 V s^{-1}, and 0.1 M $KClO_4$ was used as the electrolyte solution.

Due to the enhanced surface area, the honeycomb gold arrays can serve as excellent substrates for the development of electrochemical sensors to promote electron transfer reactions between the redox species with the underlying electrode. Fig. 4 shows cyclic voltammograms acquired at the bare gold electrode (curve a) and the honeycomb gold arrays electrode (curve b, c, d) after immersing the electrodes in an ethanol solution containing 1 mM 6-Ferrocenyl-1-hexanethiol. Curve b, c and d in Fig. 4 correspond to the electrochemical responses at the metal arrays formed at deposition potentials of -0.1 V in 10 mM $HAuCl_4$ (honeycomb gold arrays with a thickness of 410 nm), -0.8 V in 2.5 mM $HAuCl_4$ (honeycomb gold arrays with a thickness of 420 nm) and -0.8 V in 10 mM $HAuCl_4$ (honeycomb gold arrays with a thickness of 598 nm), respectively. At the bare gold electrode, the anodic peak potential (E_{pa}) is 0.380V, while E_{pa} shifts negatively in the case of the gold arrays electrode. The peak current at the honeycomb gold arrays electrode is about 2.7 times (curve b), 2.7

times (curve c) and 4.3 times (curve d) greater than that shown in curve a, which indicates that the honeycomb gold arrays electrode possesses excellent sensitivity towards 6-Ferrocenyl-1-hexanethiol.

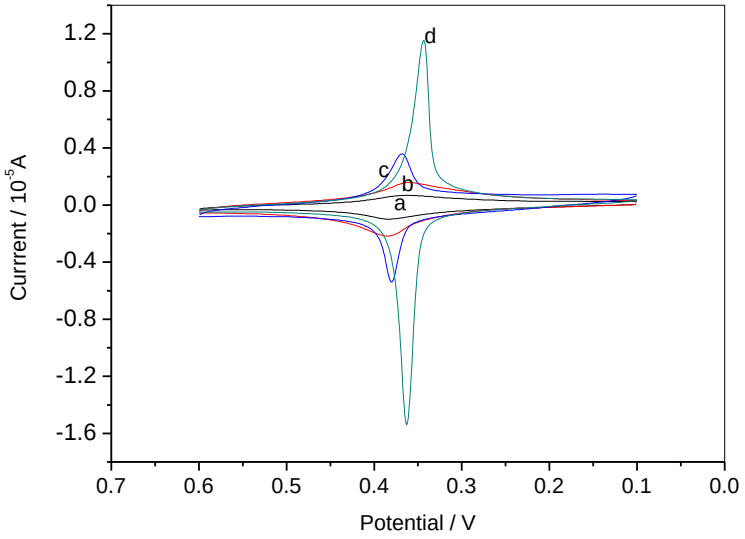

Figure 5. Cyclic voltammograms acquired at the bare gold electrode (curve a, c) and the honeycomb gold arrays electrode (curve b, d) after immersing the electrodes in an ethanol solution containing different 6-Ferrocenyl-1-hexanethiol concentration. Curve a and b: 0.1 mM 6-Ferrocenyl-1-hexanethiol; Curve c and d: 1 mM 6-Ferrocenyl-1-hexanethiol. The scan rate was 0.05 V s^{-1}, and 0.1 M $KClO_4$ was used as the electrolyte solution.

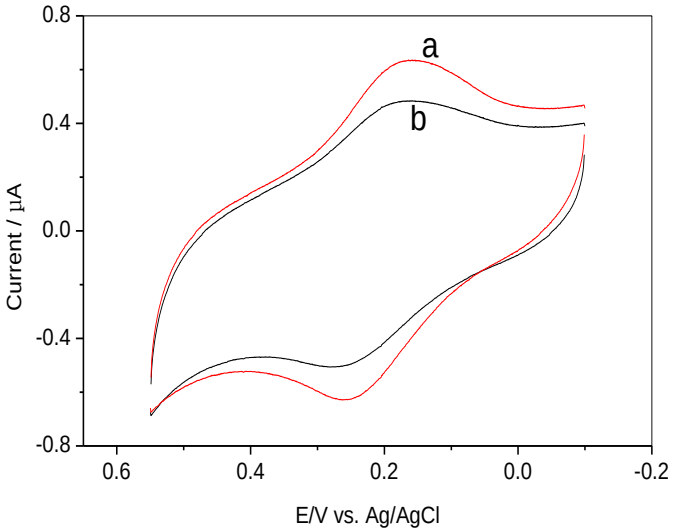

Figure 6. Cyclic voltammograms of the bare gold electrode (curve b) and the honeycomb gold arrays electrode (curve a) covered capture probe after hybridization reactions with target DNA and a detection probe attached with the Fc-Mi. The scan rate was 0.05 V s^{-1}, and 0.1 M $KClO_4$ was used as the electrolyte solution.

The high sensitivity of the honeycomb gold arrays electrode towards 6-Ferrocenyl-1-hexanethiol is attributed to the more reversible redox behavior [25] of 6-Ferrocenyl-1-hexanethiol at

this electrode. The reason for the large peak current in comparison with that at the bare electrode may originate from the large surface area at the gold arrays.

Fig. 5 demonstrates cyclic voltammograms acquired at the bare gold electrode (curve a, c) and the honeycomb gold arrays electrode (curve b, d) after immersing the electrodes in an ethanol solution containing different 6-Ferrocenyl-1-hexanethiol concentration. As shown in Fig. 5, compared with the bare gold electrode, position of the oxidation peak in the honeycomb gold arrays electrode after immersing the electrodes in an ethanol solution containing the same 6-Ferrocenyl-1-hexanethiol concentration shift negatively at least 10 mV. Besides, the peak current at the honeycomb gold arrays electrode is about 2.5 times and 2.7 times as great as that at the bare gold electrode at 0.1 mM 6-Ferrocenyl-1-hexanethiol and 1 mM 6-Ferrocenyl-1-hexanethiol, respectively. This further indicates that the honeycomb gold arrays electrode possesses more sensitive electrochemical signal towards 6-Ferrocenyl-1-hexanethiol. The peak current value at the bare gold electrode and the honeycomb gold arrays electrode related with 6-Ferrocenyl-1-hexanethiol concentration is also observed. The higher the 6-Ferrocenyl-1-hexanethiol concentration, the greater the oxidation peak current of electrode.

Fig. 6 depicts cyclic voltammograms of the bare gold electrode (curve b) and the honeycomb gold arrays electrode (curve a) covered capture probe after hybridization reactions with target DNA and a detection probe attached with the Fc-Mi. Table 1 shows peak current and peak potential of cyclic voltammograms of the bare gold electrode (curve b) and the honeycomb gold arrays electrode (curve a) covered capture probes after hybridization reactions with target DNA and a detection probe attached with the Fc-Mi. At the bare gold electrode, the anodic peak potential (E_{pa}) is 0.275 V, while E_{pa} shifts negatively 0.012 V in the case of the gold arrays.

Table 1. Peak current and peak potential of cyclic voltammograms of the bare gold electrode (curve b) and the honeycomb gold arrays electrode (curve a) covered capture probes after hybridization reactions with target DNA and a detection probe attached with the Fc-Mi.

Electrode	E_{pa}(V)	E_{pc}(V)	E_p(V)	I_{pa}(μA)	I_{pc}(μA)
Bare gold (curve b)	0.275	0.169	0.106	0.121	0.102
Honeycomb gold arrays electrode (curve a)	0.263	0.158	0.105	0.198	0.179

It can be seen from Fig. 6 and table 1 that the anodic peak current and cathodic peak at the honeycomb gold arrays are 0.198 μA and 0.179 μA, the anodic peak current and cathodic peak at the bare gold electrode are 0.121 μA and 0.102 μA, respectively. Namely, the peak current at the honeycomb gold arrays is about 1.67 times greater than that at the bare gold electrode, which demonstrates that the honeycomb gold arrays electrode possesses excellent sensitivity towards DNA hybridization reactions. This phenomenon is similar to that shown in Fig. 4. The peak current value in the honeycomb gold arrays electrode is higher than that of gold electrode modified by self-assembled monolayers of thiols to determine DNA sequences hybridization [26]. However, the peak current value in the honeycomb gold arrays electrode is lower than that of DNA hybridization via oxidation of the

ferrocene caps on the gold nanoparticle/streptavidin conjugates [27]. This can be explained as follows: the peak current value in reference [27] is calculated within the scan rate of 0.3 V s^{-1}, which is higher than that in this work (0.05 V s^{-1}). The higher the scan rate, the higher the peak current. Meanwhile, sequences of detection probes and the target DNA in reference [27] are different from those in our work. Moreover, peak current value in the honeycomb gold arrays is not the high when compared with literature about electrochemical detection of DNA hybridization [28]. This is ascribable to higher concentration of capture DNA in literature [28] and different sequences of DNA.

4. CONCLUSIONS

Honeycomb gold arrays were fabricated via gold electrodeposition within the interstitial voids of hexagonally close-packed PS nanospheres on gold films. The thickness of the metal arrays depends largely on the deposition potential and the plating solution concentration. With the deposition potential of -0.8 V and the plating solution of 10 mM $HAuCl_4$, a thickness of 598 nm of the honeycomb gold arrays on gold films is obtained. Alteration of the potential to -0.1 V results in a thinckness of 410 nm of gold arrays on gold films. In the case of 2.5 mM $HAuCl_4$ and the deposition potential of -0.8 V, the thickness of the honeycomb gold arrays is about 420 nm on gold films. The metal arrays remain uncollapsed after extraction of PS cores with toluene and the size of the arrays is controlled by the diameter of the PS nanospheres assembled on the surface. Due to the enhanced surface area, the metal arrays can be used as electrochemical sensors to promote electron transfer reactions between the redox species with the underlying electrode and used in DNA analysis to improve sensitivity of DNA hybridization reactions.

ACKNOWLEDGEMENTS
This work is supported financially by National Natural Science Foundation of China (No. 51272032) and the Postdoctoral Science Foundation of Central South University.

References

1. J. Zhang, C.M. Li, *Chem. Soc. Rev.*, 41 (2012) 7016.
2. S. Nishimura, A. Shishido, N. Abrams, T.E. Mallouk, *Appl. Phys. Lett.*, 81 (2002) 4532.
3. B.R. Duan, Q. Cao, *Electrochim. Acta*, 64 (2012) 154.
4. X.H. Xia, J.P. Tu, X.L. Wang, C.D. Gu, X.B. Zhao, *J. Mater. Chem.*, 21 (2011) 671.
5. X.H. Xia, J.P. Tu, J. Zhang, X.H. Huang, X.L. Wang, X.B. Zhao, *Electrochim. Acta*, 55 (2010) 989.
6. R.G. Shimmin, R. Vajtai, R.W. Siegel, P.V. Braun, *Chem. Mater.*, 19 (2007) 2102.
7. M. Gamero, M. Sosna, F. Pariente, E. Lorenzo, P.N. Bartlett, C. Alonso, *Talanta*, 94 (2012) 328.
8. M. Sadakane, K. Sasaki, H. Kunioku, B. Ohtani, R. Abe, W. Ueda, *J. Mater. Chem.*, 20 (2010) 1811.
9. Stéphane Reculusa, Béatrice Agricole, Alain Derré Michel Couzi, Elisabeth Sellier, Pierre Delhaès, Serge Ravaine, *Electroanalysis*, 19 (2007) 379.
10. B. Sakintuna, Y. Yürüm, *Ind. Eng. Chem. Res.*, 44 (2005) 2893.
11. Y.C. Lee, T.J. Kuo, C.J. Hsu, Y.W. Su, C.C. Chen, *Langmuir*, 18 (2002) 9942.

12. P. Jiang, K.S. Hwang, D.M. Mittleman, J.F. Berton, V.L. Colvin, *J. Am. Chem. Soc.*, 121 (1999) 11630.
13. K.M. Kulinowski, P. Jiang, H. Vaswani, V.L. Colvin, *Adv. Mater.*, 12 (2000) 833.
14. G.S. Attard, P.N. Bartlett, N.R.B. Coleman, J.M. Elliott, J.R. Owen, J.H. Wang, *Science*, 278 (1997) 838.
15. C.W. Chen, T. Serizawa, M. Akashi, *Chem. Mater.*, 11 (1999) 1381.
16. J.D. Qiu, H.Z. Peng, R.P. Liang, M. Xiong, *Electroanalysis*, 19 (2007) 1201.
17. Y. Bai, W. Yang, Y. Sun, C. Sun, *Sensor and Actuat. B-Chem.*, 134 (2008) 471.
18. C.H. Wang, C. Yang, Y.Y. Song, W. Gao, X.H. Xia, *Adv. Funct. Mater.*, 15 (2005) 1267.
19. Y.Y. Song, Y. Li, C. Yang, X.H. Xia, *Anal. Bioanal. Chem.*, 390 (2008) 333.
20. X. Chen, Y. Wang, J. Zhou, W. Yan, X. Li, J.-J. Zhu, *Anal. Chem.*, 80 (2008) 2133.
21. X.H. Li, L. Dai, Y. Liu, X.J. Chen, W. Yan, L.P. Jiang, J.J. Zhu, *Adv. Funct. Mater.*, 19 (2009) 3120.
22. A.J. Bard, L.R. Faulkner, Electrochemical Methods: Fundamentals Applications, John Wiley & Sons, New York, 2001.
23. K. DiGleria, C.M. Halliwell, C. Jacob, H.A.O. Hill, *FEBS Lett.*, 400 (1997) 155.
24. H. Martin, P. Carro, A.H. Creus, S. Gonzáez, G. Andreasen, R.C. Salvarezza, A.J. Arvia, *Langmuir*, 16 (2000) 2915.
25. C.R. Raj, T. Okajima, T. Ohsaka, *J. Electroanal. Chem.*, 543 (2003) 127.
26. M.M.S. Silva, I.T. Cavalcanti, M.F. Barroso, M.G.F. Sales, R.F. Dutra, *J. Chem. Sci.*, 122 (2010) 911.
27. J. Wang, J. Li, A.J. Baca, J. Hu, F. Zhou, W. Yan, D.W. Pang, *Anal. Chem.*, 75 (2003) 3941.
28. G. Li, X. Li, J. Wan, S. Zhang, *Biosens. Bioelectron.*, 24 (2009) 3281.